Physica D 309 (2015) 1–8

Contents lists available at ScienceDirect

Physica D

journal homepage: www.elsevier.com/locate/physd

Dynamics and statistics of noise-like pulses in modelocked lasers

Graham M. Donovan

Department of Mathematics, University of Auckland, Private Bag 92019, Auckland 1142, New Zealand

HIGHLIGHTS

- Noise-like pulses are an optical phenomenon that consist of chaotic pulse bunches.
- These form a stable envelope with a fluctuating internal structure.
- These noise-like pulses can occur in mode locked laser systems.
- They may emerge from soliton-like mode locking by different dynamic mechanisms.
- The statistics may be near-Gaussian, or heavy-tailed.

ARTICLE INFO

Article history:
Received 28 January 2015
Received in revised form
13 July 2015
Accepted 14 July 2015
Available online 21 July 2015
Communicated by V.M. Perez-Garcia

Keywords:
Extreme events
Bifurcations
Optical rogue waves
Polarization controller

ABSTRACT

Noise-like pulses and optical rogue waves are connected nonlinear phenomena which can occur in passively modelocked laser systems. Here we consider a range of model systems to explore the conditions under which noise-like pulses can be expected to occur, and further when the resulting statistics meet the optical rogue wave criteria. We show, via a series of careful simulations, that noise-like pulses and optical rogue waves can arise either separately or together, and that they may emerge from standard soliton-like solutions via different mechanisms. We also propose a quantitative definition of noise-like pulses, and explore the issues carefully in convergence testing numerical methods for such systems.

1. Introduction

Noise-like pulses (NLPs) are a phenomenon observed in optical systems (both experimental and theoretical) wherein a chaotic pulse bunch forms a stable temporal envelope with a fluctuating internal structure (e.g. [1–4]). This often occurs as a bifurcation in systems which also exhibit stable single-pulse solutions, and the NLP statistics may either be Gaussian, or heavy-tailed [5,6]. If the distributions are sufficiently heavy-tailed, they may meet the criteria to be considered optical rogue waves (ORWs) [4].

Optical rogue waves are rare, large amplitude events in optical systems. They have recently gained much attention, both theoretical and experimental [7,8], in part because of potential parallels with oceanic rogue waves. Although questions remain about how much insight can be gained into ocean rogue waves from their optical cousins, optical rogue waves (ORWs) are nonlinear phenomena of interest in their own right. In particular we look here at rogue waves in laser systems, which differ in important ways from those originally observed by Solli et al. [7]. Here the system is no longer conservative, because of gain and loss in the laser cavity, and so some of the potential connections with oceanic waves have been lost [9]. Still, the term "rogue wave" is widely used in such systems, and here we consider the origins, dynamics and statistics of such laser rogue waves. The concepts of ORWs and NLPs are connected by the fact that some NLPs meet the criteria to be considered rogue waves [4], though of course ORWs can arise by other mechanisms.

Here we consider the dynamic origins of noise-like pulses in passively modelocked laser systems, and also their statistics and role as generators of ORWs. We first consider a generic formulation and outline the method of study; then we consider several example systems drawn from the literature. Each of these systems is selected to consider the role of one or more (potentially) important system characteristics. We show that NLPs can emerge from the single-pulse solution in several different ways; that they can occur in either normal or anomalous dispersion systems; in either one or two polarization systems; and with an explicit or lumped modelocking mechanism. Further, our examples demonstrate that from this set of trial systems, no single characteristic is sufficient to predict the character of the pulse amplitude statistics *a priori*. As part of this analysis we propose a quantitative definition of NLPs in these systems.

E-mail address: g.donovan@auckland.ac.nz.

http://dx.doi.org/10.1016/j.physd.2015.07.003
0167-2789/

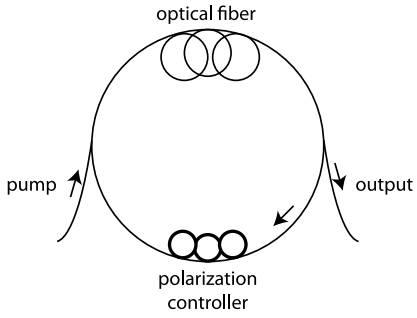

Fig. 1. Schematic illustration of sample passively mode-locked laser system.

One significant challenge in studying NLPs in modelocked lasers is reproducibility of existing studies. Here we provide full, explicit and complete descriptions of the models and numerical methods used, as well as demonstrations of numerical convergence (particularly near the chaotic attractors).

2. Models

We begin by considering a nonlinear polarization evolution (NPE) modelocked laser in its most general terms: a laser cavity which consists of optical fibre (including gain media) and a polarization controller (PC); see Fig. 1. Propagation of light through the fibre is described by the cubic nonlinear Schrödinger equation (NLS), or one of its variants, while the PC is a discrete element. The combination must effectively act as a saturable absorber. The system is said to be mode-locked if a stable solution, modulo phase rotation, emerges after some (possibly very large) number of round trips.

If we take a section through one location in the cavity (e.g. at the output coupler), and discretize the PDE, then the models we consider are iterated maps

$$f : \mathbb{C}^N \to \mathbb{C}^N$$

where each iteration of the map corresponds to a single round trip of the laser cavity. Then a modelocked solution can be thought of as an invariant set of this iterated map.

As a simple example, one might consider a single piece of gain fibre, with one polarization, and a lumped polarization controller. Then the governing equations are given by the NLS with saturating gain

$$i\frac{\partial u}{\partial z} + \frac{D}{2}\frac{\partial^2 u}{\partial t^2} + \gamma|u|^2 u = G(z)u \tag{1}$$

for propagation in the fibre, where

$$G(z) = \frac{g_0}{1 + (1/E_0)\int_{-\infty}^{\infty}|u|^2 dt}, \tag{2}$$

paired with a lumped saturable absorber

$$u_{out}(t) = u_{in}(t)\exp\left(-\frac{\Delta}{2\left(1 + |u|^2/P_{sat}\right)}\right). \tag{3}$$

Here $u(t, z)$ is the propagating light (with the optics convention of z as the propagation direction), D as the fibre dispersion, γ the fibre nonlinearity, g_0 the small signal gain, E_0 the gain saturation energy, Δ the modulation depth of the saturable absorber, and P_{sat} is the saturation power.

Then propagation through the fibre, combined with the discrete element, forms the action of f. Of course the systems we consider in detail differ somewhat, but we present this minimal formulation here to illustrate the model concept. Here we have used a lumped saturable absorber, wherein the action of the whole NPE is taken with a single empirical element (Eq. (3)). We will also consider systems where all the physical elements of the NPE are explicitly modelled, and we refer to this as an explicit NPE—for full details, see Appendix A.

We can then consider the behaviour of the laser by studying the dynamics of this iterated map; in general we consider a single bifurcation parameter associated with the gain of the system. For "small" values of the bifurcation parameter we might expect to see single, stable pulse modelocking (solitons, or soliton-like). As the parameter is increased, more complex modelocking can occur, including noise-like pulses.

The example systems we consider are variations on this theme. Complete descriptions and references are given in the following sections and Appendix A. In short, we consider example system to explore the roles of several important system characteristics and modelling choices:

- optical fibre dispersion: normal or anomalous dispersion
- standard or coupled NLS (one polarization or two)
- polarization controller (NPE) model: explicit or lumped.

Details of each model system are provided in the following sections.

3. Results

3.1. Soliton solutions, invariant sets, and bifurcations

In general, for "small" values of the bifurcation parameter, the system mode-locks to a single, stable pulse which may be a soliton, or soliton-like (if mode-locking occurs at all). However, one must be aware of the difference between observed optical mode locking, which measures $|u(t)|^2$, and the iterated map in $u(t)$; because of the phase rotation, even this simple mode-locking regime does not yield an equilibrium, but rather an invariant set. (Fortunately, the governing equations are also phase invariant in general.) Typically the soliton-like solution for small gain is found simply by iterating the map numerically from a small, white-noise seed. From there continuation is employed to generate bifurcation diagrams; either naive continuation where possible, or more sophisticated methods where required—see Appendix B for more details.

3.2. Models

We begin by considering three models drawn from the literature, chosen to explore the influence of dispersion (normal vs. anomalous), polarization, and NPE modelling type. These models are:

1. The normal dispersion, two polarization, explicit PC model of Zaytsev et al. [10].
2. The normal dispersion, single polarization, lumped PC model of Zaviyalov et al. [11].
3. The anomalous dispersion, single polarization, lumped PC model of Soto-Crespo et al. [12].

We further create a fourth model by hybridizing the first and second listed above, in the sense of converting the explicit NPE of case 1 into a lumped NPE, so that we also have a model with normal dispersion, a lumped PC, and two polarizations.

In each case we have calculated steady state solutions, (partial) bifurcation diagrams, and evolution statistics to test for optical rogue waves. The details of each case are presented in the following sections.

3.2.1. Normal dispersion, two polarizations, explicit PC

We first consider the model of Zaytsev et al. [10], which features normal dispersion, two polarizations, and an explicit PC model. The bifurcation parameter here is the gain saturation energy E_{sat}, and we begin by computing the bifurcation diagram for E_{sat} ranging

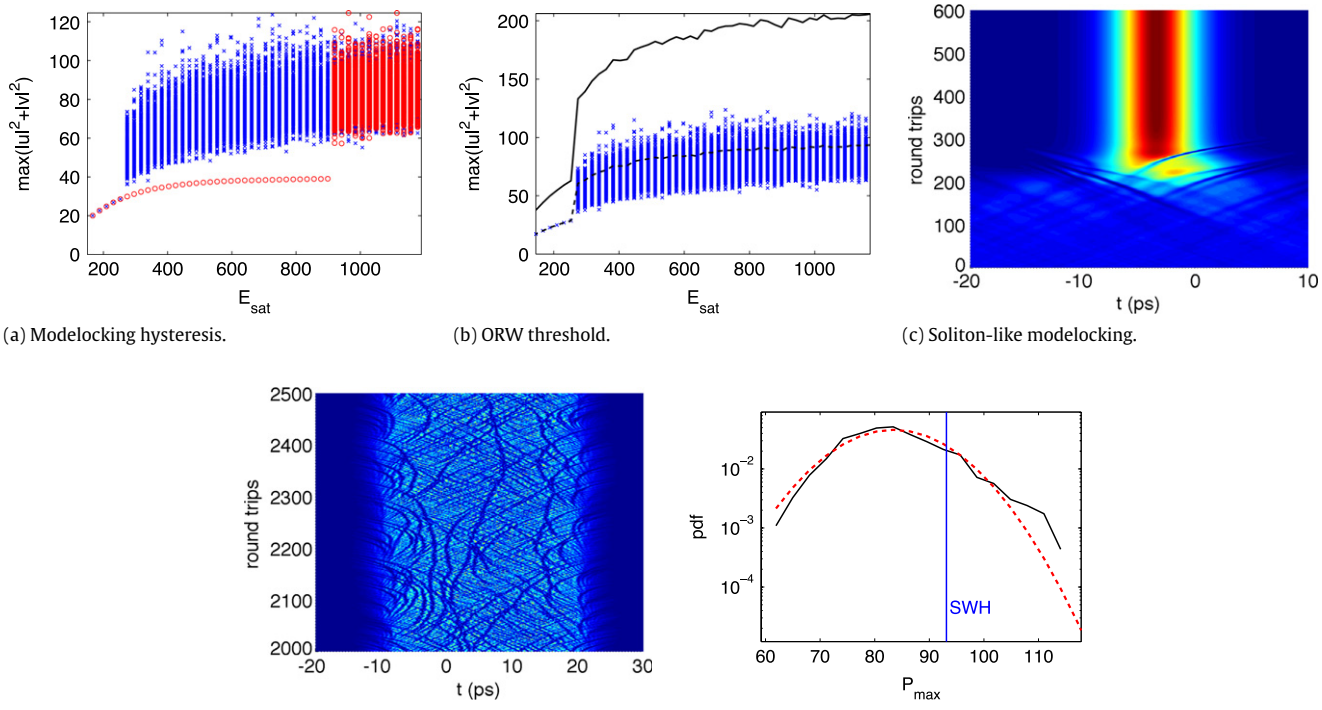

(a) Modelocking hysteresis. (b) ORW threshold. (c) Soliton-like modelocking.

(d) NLP detail. (e) Near-Gaussian statistics.

Fig. 2. Simulation results from the model of Zaytsev et al. [10]. Panel (a) gives the bifurcation diagram and illustrates the co-existence of soliton-like and NLP solutions, with the red circles giving solution amplitudes while increasing the bifurcation parameter, and the blue crosses in the decreasing case. Panel (b) overlays the decreasing branch with the significant wave height (SWH), black dashed curve, and the rogue wave threshold (2.2 times SWH), solid dashed curve. Panel (c) gives an illustrative profile of modelocking to a soliton-like solution ($E_{sat} = 145$ pJ), and panel (d) gives detail of a noise-like pulse ($E_{sat} = 1000$ pJ). Panel (e) compares the maximum amplitude statistics of a noise like pulse (black curve, $E_{sat} = 1000$ pJ) with the best-fit Gaussian (dashed red). The SWH threshold is also given; note that the ORW threshold of 2.2 times SWH is well off-axis. (For interpretation of the references to color in this figure legend, the reader is referred to the web version of this article.)

from 145 to 1200 pJ, shown in Fig. 2(a). The red circles give the continuation path for increasing E_{sat}, beginning with a stable, soliton-like solution 2(c) and changing into a noise-like pulse for $E_{sat} \sim$ 950 pJ 2(d), in agreement with the findings of [10]. The system is hysteretic in the sense that there is a broad region of coexistence of both soliton and noise-like solutions, depending on the initial conditions. We illustrate this by continuing in the negative ΔE_{sat} direction, back from 1000 to 145 pJ; these solutions are given by the blue crosses in 2(a). Thus from approximately 300 to 950 pJ, both solution types coexist. Above and below this, only one is possible.

We consider the statistics of these noise-like pulses, in particular the variation in peak intensity with each round trip. In particular we are interested in classifying the high-intensity tail of the distribution (so-called *L-shaped* statistics), and to do so we use the established criteria in terms of the significant wave height (SWH) or significant intensity [11,13]. The SWH is defined as the mean of the upper third of wave heights, and then ORWs as waves exceeding 2.2 times the SWH.[1] In 2(b) we give both the SWH and the ORW threshold, as the dashed and solid lines, respectively; at no value of E_{sat} are there amplitudes above the ORW threshold. In fact, the distributions are relatively close to Gaussian—see 2(e) as an illustration at $E_{sat} = 1000$ pJ, along with the Gaussian matched to the sample mean and variance.

In short, this model yields clear noise-like pulses in a normally dispersive regime (the dark solitons are clear in the evolution of both solutions, 2(c) and (d)), but the statistics of these solutions are near Gaussian and far from optical rogue waves. There is also a significant region of co-existence between soliton-like pulses, and NLP operation.

[1] Some authors define the ORW threshold as 2 times the SWH.

3.2.2. Normal dispersion, single polarization, lumped PC

We next consider the model of Zaviyalov et al. [11] with normal dispersion, one polarization, and a lumped PC model. The bifurcation parameter here is the small-signal gain g_0, and we begin by computing the bifurcation diagram for g_0 ranging from 0.4 to 2.4 (m^{-1}), shown in Fig. 3(a). This solution loses stability at $g_0 \sim 0.41$ (m^{-1}) and the quasi-periodic solution that emerges is illustrated in 3(c).

As the gain is increased, more complex solutions emerge, e.g. Fig. 3(d), and now optical rogue waves occur. We again calculate the SWH and ORW threshold, given in 3(a) as the dashed and solid black lines respectively. It is clear that ORWs do occur, and their observed probabilities are given in 3(b); the distribution of peak amplitudes for $g_0 = 2$ (m^{-1}) is given in 3(e), along with a best fit Gaussian for comparison—clearly large amplitude events occur much more often than predicted by Gaussian statistics. The solutions which give rise to these heavy-tailed statistics are perhaps chaotic, but they do not qualify as noise-like pulses according to our definition (see Section 3.3). Thus, in this model, again a clearly normal dispersion regime with clear dark solitons, optical rogue waves do occur, but without noise-like pulses. It is also noteworthy that the dynamics are entirely different, with the original soliton-like solution losing stability, and the occurrence of quasi-periodic solutions before these give way to chaotic solutions. There is no region of co-existence between soliton-like and more complex solutions.

3.2.3. Anomalous dispersion, single polarization, lumped PC

Up to this point we have considered only normally dispersive systems; here we examine the anomalous dispersion model of Soto-Crespo et al. [12]. This model employs a single polarization and a lumped NPE. The loss of stability occurs via a period-doubling cascade, and optical rogue waves occur in the chaotic regime (as

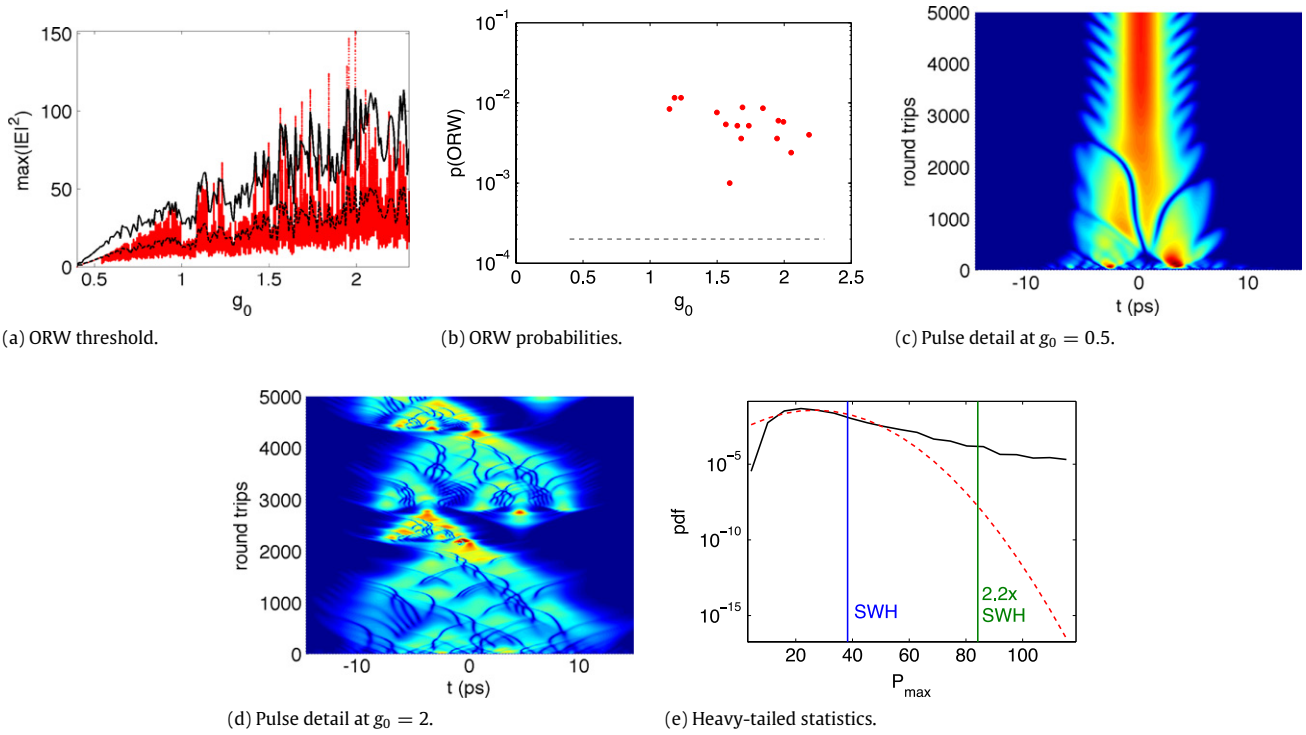

(a) ORW threshold. (b) ORW probabilities. (c) Pulse detail at $g_0 = 0.5$.

(d) Pulse detail at $g_0 = 2$. (e) Heavy-tailed statistics.

Fig. 3. Simulation results from the model of Zaviyalov et al. [11]. Panel (a) gives the maximum amplitude as the parameter g_0 is varied, with significant wave height (SWH), black dashed curve, and the rogue wave threshold (2.2 times SWH), solid dashed curve. Panel (b) gives the optical rogue wave probability, where ORWs appeared in the sample—the black dashed line gives the minimum detectable threshold, given the sample size. Panel (c) gives an illustrative profile of a quasi-periodic solution ($g_0 = 0.5$), and panel (d) gives detail of a more complex solution ($g_0 = 2$). Panel (e) compares the maximum amplitude statistics of a noise like pulse ($g_0 = 2$, black curve) with the best-fit Gaussian (red, dashed), as well as the SWH and the ORW threshold of 2.2 times SWH. (For interpretation of the references to color in this figure legend, the reader is referred to the web version of this article.)

Table 1
Summary of model behaviour.

Model	Dispersion	NLPs	Statistics	NPE/PC	Polarizations	Co-existence[a]
Zaytsev et al.	Normal	Yes	Gaussian	Explicit	2	Yes
Zaviyalov et al.	Normal	No	ORWs	Lumped	1	No
Soto-Crespo et al.	Anomalous	Yes	ORWs	Lumped	1	No
Hybrid	Normal	Yes	Gaussian	Lumped	2	Yes

[a] Co-existence of soliton and NLP solutions for a single value of the bifurcation parameter.

demonstrated in [12]). The bifurcation parameter here is the saturation energy Q_{sat}.

Again we calculate the bifurcation diagrams, and compare the bifurcation diagram with the SWH and ORW thresholds 4(a). Example solution evolutions are given in panels 4(c)–(d), at $Q_{sat} = 2.5$ and 60 illustrating a period-2 solution, and a noise-like pulse respectively. Here there is no co-existence of solutions, with the soliton-like solution losing stability through a period-doubling cascade. The chaotic, bunched solutions which emerge in bands for higher Q_{sat} are noise-like pulses according to our criterion (see Section 3.3).

The observed ORW probabilities are given as Q_{sat} varies in 4(b). There are clearly significant regions where the probability of large amplitudes meets the ORW test, and these correspond to the regions of noise-like pulses. The statistics of these solutions are explored in some detail in the original paper [12].

3.2.4. Normal dispersion, two polarization, lumped PC

The models considered so far have been drawn from the literature to examine the role of dispersion, NPE model type, and birefringence on both NLP and ORW formation. The suggestion from this limited sample is that ORWs might occur in either lumped PC systems, or single polarization systems. To explore further, we construct a hybrid system, by taking system 1 (Normal dispersion, two polarizations, explicit PC from [10]) and modifying by reducing the explicit NPE to a lumped model as follows

$$\begin{bmatrix} u_{out} \\ v_{out} \end{bmatrix} = \exp\left(-\frac{1}{2} \frac{\delta_0 \Delta z}{1 + \frac{|u|^2 + |v|^2}{P_{sat}}} \right) \begin{bmatrix} u \\ v \end{bmatrix} \tag{4}$$

where the modulation depth $\delta_0 \Delta z = 2$ and $P_{sat} = 321$ W (modified from [11]). We maintain the Gaussian filter as in the original description (see Appendix A).

This model continues to exhibit NLPs, and these have (near) Gaussian statistics. The coexistence hysteresis loop between soliton-like operation and NLPs is given in Fig. 5(a) and (b) using simple ramping of the parameter [14]. The distribution of amplitudes at $E_{sat} = 500$ nJ is given in 5(c) along with a best-fit Gaussian for comparison.

Thus the hybridized model exhibits NLPs with Gaussian statistics, with co-existence of NLPs and standard modelocking. The properties of the models considered in the preceding sections are concisely summarized in Table 1.

3.3. Defining noise-like pulses

Noise-like pulses are often defined qualitatively by an autocorrelation with a narrow peak on a broad base. We propose a quan-

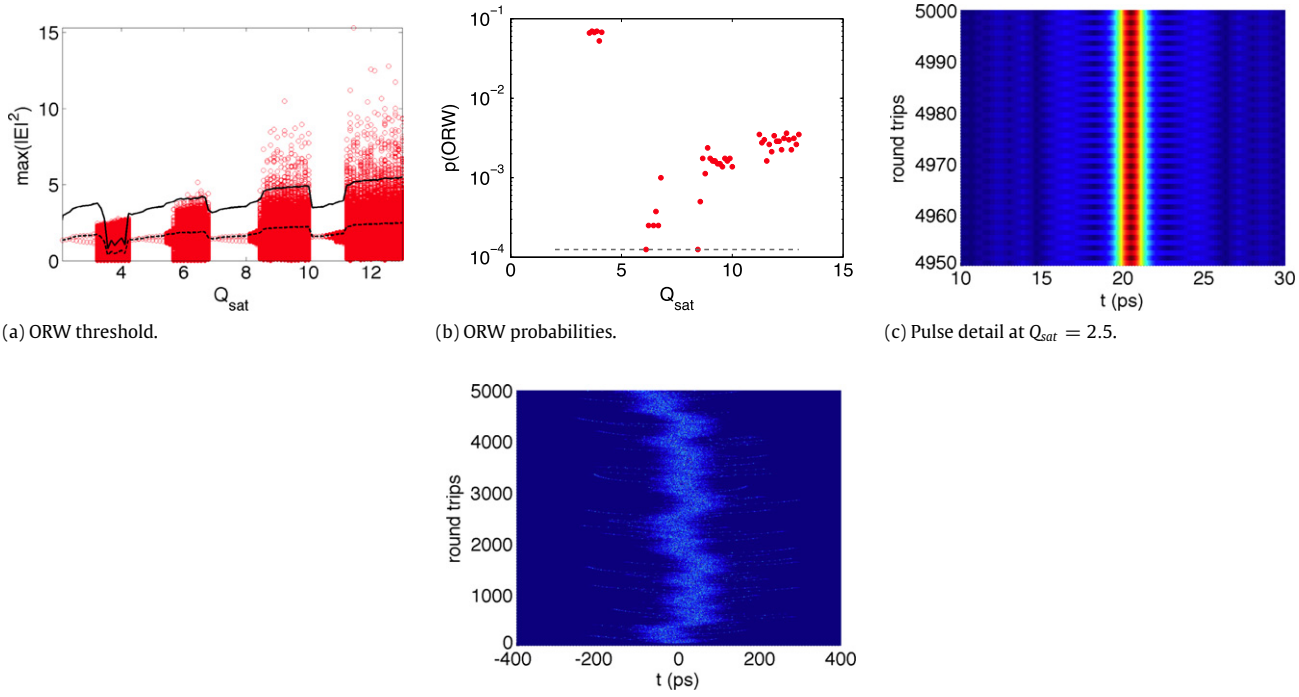

(a) ORW threshold. (b) ORW probabilities. (c) Pulse detail at $Q_{sat} = 2.5$.

(d) Pulse detail at $Q_{sat} = 60$.

Fig. 4. Simulation results from the model of Soto-Crespo et al. [12]. Panel (a) gives the maximum amplitude as the parameter Q_{sat} is varied, with significant wave height (SWH), black dashed curve, and the rogue wave threshold (2.2 times SWH), solid dashed curve. Panel (b) gives the optical rogue wave probability, where ORWs appeared in the sample—the black dashed line gives the minimum detectable threshold, given the sample size. Panel (c) gives an illustrative profile of a period-2 solution ($Q_{sat} = 2.5$), and panel (d) gives detail of a noise-like pulse ($Q_{sat} = 60$).

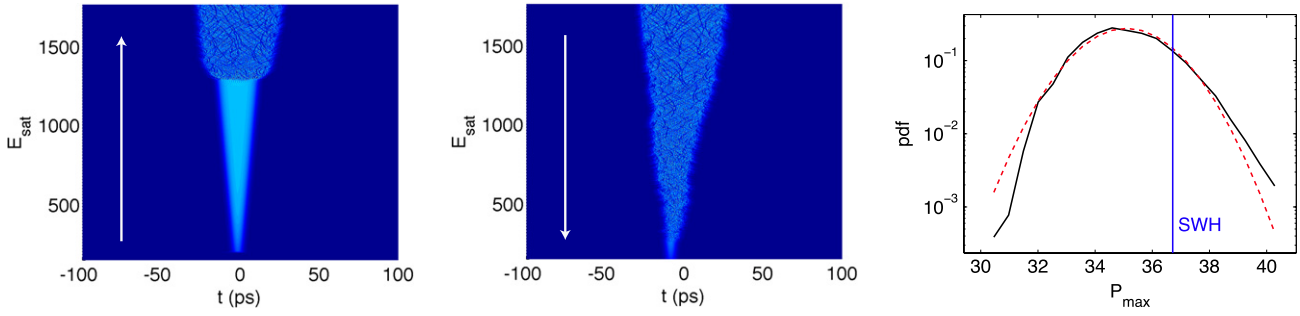

(a) Increasing E_{sat}. (b) Decreasing E_{sat}. (c) Near-Gaussian statistics.

Fig. 5. Simulation results from the hybrid model. Panels (a) and (b) illustrate the co-existence of soliton-like and NLP solutions, with (a) giving the profile while increasing the bifurcation parameter, and (b) the decreasing case. Panel (c) compares the maximum amplitude statistics of a noise like pulse ($E_{sat} = 1000$ pJ, black curve) with the best-fit Gaussian (red, dashed). The SWH threshold is also given; note that the ORW threshold of 2.2 times SWH is well off-axis. (For interpretation of the references to color in this figure legend, the reader is referred to the web version of this article.)

titative definition based on widths of the autocorrelation, as

$$\sigma = \frac{FW_{75}}{FW_{25}} \tag{5}$$

where $FW_{75/25}$ are the full widths at 75% and 25% of maximum, respectively. We then define noise-like pulses as those where $\sigma < 1/50$, that is, a minimum ratio of 50 between peak narrowness and base width. Fig. 6 illustrates the concept using the autocorrelation of pulses studied here; using this definition, all models except that of Zaviyalov et al. have solutions which we classify as NLPs.

4. Discussion

We have shown, through careful simulation, that the related phenomena of noise-like pulses and optical rogue waves can occur in a variety of passively modelocked laser systems. From these few systems we hoped that some simple criteria for formation of

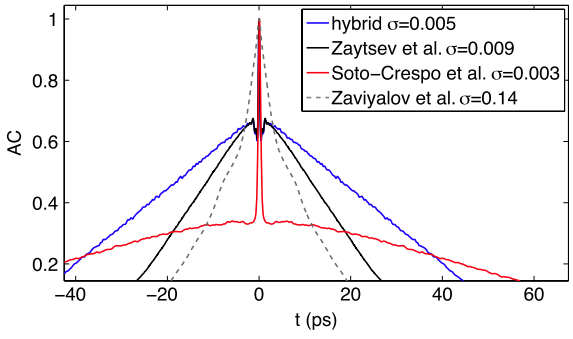

Fig. 6. Autocorrelations for complex pulses, given for comparison with the proposed definition of a noise-like pulse. With a threshold of $\sigma < 1/50$, all but the model of Zaviyalov et al. qualify as NLPs.

NLPs and/or ORWs might be clear; however, it remains possible that normal dispersion NLPs always generate Gaussian statistics,

and it is not clear in what circumstances NLPs occur. We have also considered only statistics with respect to pulse amplitude, though spectral rogue waves are also of interest and may not be subject to the same system criteria as their temporal cousins [3,4].

Here we have also considered only models with discrete cavity elements, rather than averaged models which apply those effects continuously during propagation, resulting in a single governing equation which is often a variant of the complex Ginzburg Landau equation (e.g. [12,15]). Such averaged models can have significant advantages because they are so much easier to work with; however, it is not clear under what conditions the averaging procedures leave NLP dynamics intact. Of course it would be ideal to consider these systems in greater generality, whether averaged or discrete, rather than a handful of examples. However, the great challenge is that modelocking, especially for NLPs, is extremely difficult to find in model systems.

This is a combination of several factors. First is that, especially with explicit NPEs, modelocking is extremely parameter sensitive. Even small changes to waveplate angles or other system parameters can prevent modelocking altogether. This is also true in physical systems, but exploring a high-dimensional parameter space is relatively easier with physical systems, because iterations occur in the MHz range. With a computationally intensive model, on the other hand, iterations are more typically order 1 Hz, or worse. Because modelocking can also be slow, requiring many iterations, this puts simulations at a significant disadvantage in terms of exploring parameter space.

Similarly, though there are other model systems in the literature which exhibit noise-like pulses (e.g. [16–23]) we found that only the three systems considered in this paper exhibited NLPs in our simulations.[2]

It would also be desirable to make more careful calculations of the bifurcations, including precise continuation to bifurcation points, and calculation of the spectra. However, computational cost is again a significant obstacle. Typically 2^{16} or more Fourier modes are required to fully resolve the complex waveforms, and at those levels brute-force numerical calculation of eigenvalues was found to be impractical. A more detailed discussion of the numerical and convergence issues is given in Appendix B.

In order to characterize NLPs quantitatively in our results we have proposed the simple heuristic on the ratio $\sigma = \frac{FW_{75}}{FW_{25}}$ in the autocorrelation to reflect the qualitative definition of a narrow peak on a broad base. Of course, the levels and ratio threshold of such a criterion are open to interpretation; for example, is 75% of the maximum in the peak, or the base? Nonetheless, we feel it is worthwhile to define precisely what it is that we mean by a noise-like pulse.

Acknowledgements

The author would like to thank Alexey Zaytsev, Thomas Murphy, Miro Erkintalo and Neil Broderick for their helpful comments and clarifications.

Appendix A. Model descriptions

We provide here a complete description of the explicit NPE model based on [10]. Ref. [15] also provides good background detail, though their model does not address NLPs.

The model we employ is as follows: the governing equations are

$$\frac{\partial u}{\partial z} = i\gamma\left(|u|^2u + \frac{2}{3}|v|^2u + \frac{1}{3}v^2u^*\right) + g(u,v)u - \frac{i}{2}\beta_2\frac{\partial^2 u}{\partial t^2} \tag{A.1}$$

$$\frac{\partial v}{\partial z} = i\gamma\left(|v|^2v + \frac{2}{3}|u|^2v + \frac{1}{3}u^2v^*\right) + g(u,v)v - \frac{i}{2}\beta_2\frac{\partial^2 v}{\partial t^2} \tag{A.2}$$

where $g(u,v) = g_0 \Big/ \left[1 + \int_{-T}^{T}\left(|u|^2 + |v|^2\right)dt/E_{sat}\right]$.

There are three sections of optical fibre. The first section is single mode fibre (SMF) with length 4 m, $\gamma = 0.0047\ (\mathrm{W-m})^{-1}$, $\beta_2 = 0.023\ \mathrm{ps}^2/\mathrm{m}$ and $g_0 = 0$. The second section is Yb-doped gain fibre (YDF) with length 2 m, $\gamma = 0.0016\ (\mathrm{W-m})^{-1}$, $\beta_2 = 0.023\ \mathrm{ps}^2/\mathrm{m}$ and $g_0 = 6.9$. The third section is SMF, with length 0.5 m and parameters as in the first section.

The explicit NPE is as follows: half wave plate (HWP), quarter wave plate (QWP), polarization beam splitter (PBS), differential delay line (DDL), filter, QWP.

The action of the first three elements are taken as[3]

$$\begin{aligned} u_{out}(t) = {} & \cos(2\phi)(((\cos(\theta))^2 + i(\sin(\theta))^2)u \\ & + (1-i)\sin(\theta)\cos(\theta)v) \\ & + \sin(2\phi)((1-i)\sin(\theta)\cos(\theta)u \\ & + ((\sin(\theta))^2 + i(\cos(\theta))^2)v) \end{aligned}$$

$$v_{out}(t) = 0$$

where $\phi = 0.5$ and $\theta = 1$.

The delay line is implemented as

$$u_{out} = \mathcal{F}^{-1}\left[\exp((i/2)\omega^2\rho)\mathcal{F}[u]\right] \tag{A.3}$$

$$v_{out} = \mathcal{F}^{-1}\left[\exp((i/2)\omega^2\rho)\mathcal{F}[v]\right] \tag{A.4}$$

with $\rho = 0.105\ \mathrm{ps}^2$.

The filter is also applied in the Fourier domain, with transfer function

$$\exp\left(-\frac{\sqrt{\log(2)}}{2\pi}(5.4)^{-1}\omega\right) \tag{A.5}$$

for ω in units ps^{-1}.

A loss is imposed as

$$u_{out} = 0.3u$$
$$v_{out} = 0.3v$$

and the final QWP by

$$\begin{bmatrix} u_{out} \\ v_{out} \end{bmatrix} = \begin{bmatrix} \cos(\phi_2)^2 + i\sin(\phi_2)^2 & (1-i)\sin(\phi_2)\cos(\phi_2) \\ (1-i)\sin(\phi_2)\cos(\phi_2) & \sin(\phi_2)^2 + i\cos(\phi_2)^2 \end{bmatrix} \times \begin{bmatrix} u \\ v \end{bmatrix} \tag{A.6}$$

with $\phi_2 = 0.5$.

The models of [12,10] are described fully in those citations.

[2] Because of the extreme sensitivity of the modelocking in parameter space, even small omissions in model details are difficult to overcome. For this reason, full and complete model details are given in Appendix A.

[3] Note that this expression differs from the standard model for HWP–QWP–PBS with angles 0.5 and 1 respectively, e.g. [15].

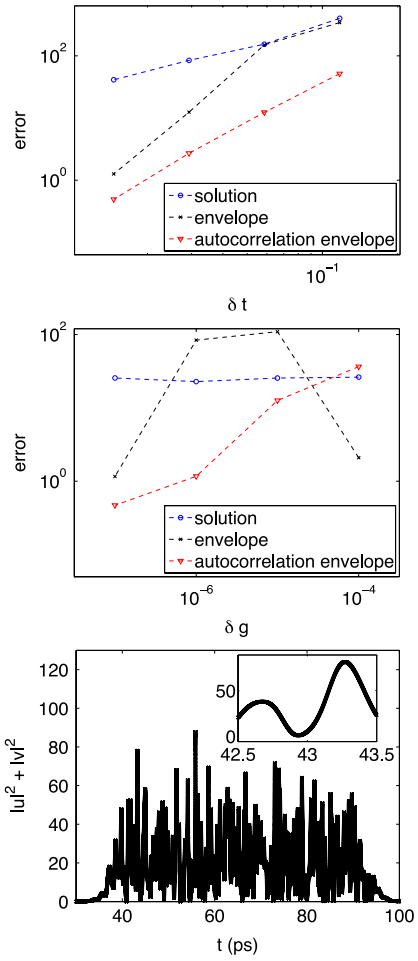

Fig. B.7. Convergence testing of numerical methods for noise-like pulses. Top panel: convergence with respect to δt. Centre panel: convergence with respect to δg, the variable stepping control parameter [25]. Bottom panel: illustration of grid scale relative to NLP scale, with each spatial point plotted explicitly, and detail given in the inset.

Appendix B. Numerical methods and convergence

For numerical solution of the fibre propagation equations we transform Eqs. (A.1)–(A.2) into

$$\frac{\partial U}{\partial z} = i\frac{\gamma}{3}\left(2|U|^2 + 4|V|^2\right)U + g(U,V)U - \frac{i}{2}\beta_2\frac{\partial^2 U}{\partial t^2} \tag{B.1}$$

$$\frac{\partial V}{\partial z} = i\frac{\gamma}{3}\left(2|V|^2 + 4|U|^2\right)V + g(U,V)U - \frac{i}{2}\beta_2\frac{\partial^2 V}{\partial t^2} \tag{B.2}$$

via the transformation

$$\begin{bmatrix} U \\ V \end{bmatrix} = \frac{1}{\sqrt{2}}\begin{bmatrix} 1 & i \\ i & 1 \end{bmatrix}\begin{bmatrix} u \\ v \end{bmatrix} \tag{B.3}$$

and then apply the standard split-step Fourier method[4] [24].

For accuracy and computational efficiency we employ the variable timestepping method of [25]. Numerical convergence was carefully tested, especially for the solutions near chaotic attractors (e.g. NLPs). Though tracking such trajectories is notoriously difficult [26], we propose using the autocorrelation envelope as convergence measure, as this is the determinant of NLPs. Convergence results are given in Fig. B.7, with the left panel giving convergence with respect to δt, the centre panel with respect to the stepping control parameter δg (see [25]), and the right panel illustrating the scale of the NLP structure relative to the numerical grid.

Domain sizes and spectral discretizations are as follows: for the model of [10] we employed a spatial domain of width 200 ps and 2^{17} spectral/time points, and also for the hybrid model. For [12], 800 ps and 2^{16}, and for [11], 120 ps and 2^{13}. In all cases the adaptive stepping tolerance δg (see [25]) was 10^{-5} or smaller. Particularly for NLPs it is important that the high-frequency components of the solution are not grid-scale (see Fig. B.7, right panel), and that the instability is physical rather than numerical.

Autocorrelations were calculated efficiently [27] via the Fourier transform as

$$\mathcal{F}^{-1}\left[\mathcal{F}\left[|u|^2 + |v|^2\right]\left(\mathcal{F}\left[|u|^2 + |v|^2\right]\right)^*\right]. \tag{B.4}$$

Initial conditions were taken to be random white noise seeds.

[4] Observe, in the splitting into linear and nonlinear parts, that the gain here is a nonlinear term.

References

[1] M. Horowitz, Y. Barad, Y. Silberberg, Noiselike pulses with a broadband spectrum generated from an erbium-doped fiber laser, Opt. Lett. 22 (11) (1997) 799–801.
[2] C. Lecaplain, Ph. Grelu, J.M. Soto-Crespo, N. Akhmediev, Dissipative rogue waves generated by chaotic pulse bunching in a mode-locked laser, Phys. Rev. Lett. 108 (23) (2012) 233901.
[3] Antoine F.J. Runge, Claude Aguergaray, Neil G.R. Broderick, Miro Erkintalo, Coherence and shot-to-shot spectral fluctuations in noise-like ultrafast fiber lasers, Opt. Lett. 38 (21) (2013) 4327–4330.
[4] C. Lecaplain, Ph. Grelu, Rogue waves among noiselike-pulse laser emission: An experimental investigation, Phys. Rev. A 90 (1) (2014) 013805.
[5] Marcelo G. Kovalsky, Alejandro A. Hnilo, Jorge R. Tredicce, Extreme events in the Ti: sapphire laser, Opt. Lett. 36 (22) (2011) 4449–4451.
[6] C. Lecaplain, Ph. Grelu, J.M. Soto-Crespo, N. Akhmediev, Dissipative rogue wave generation in multiple-pulsing mode-locked fiber laser, J. Opt. 15 (6) (2013) 064005.
[7] D.R. Solli, C. Ropers, P. Koonath, B. Jalali, Optical rogue waves, Nature 450 (7172) (2007) 1054–1057.
[8] N. Akhmediev, J.M. Dudley, D.R. Solli, S.K. Turitsyn, Recent progress in investigating optical rogue waves, J. Opt. 15 (6) (2013) 060201.
[9] John M. Dudley, Frédéric Dias, Miro Erkintalo, Goëry Genty, Instabilities, breathers and rogue waves in optics, Nat. Photonics 8 (10) (2014) 755–764.
[10] Alexey Zaytsev, Chih-Hsuan Lin, Yi-Jing You, Chia-Chun Chung, Chi-Luen Wang, Ci-Ling Pan, Supercontinuum generation by noise-like pulses transmitted through normally dispersive standard single-mode fibers, Opt. Express 21 (13) (2013) 16056–16062.
[11] Alexandr Zaviyalov, Oleg Egorov, Rumen Iliew, Falk Lederer, Rogue waves in mode-locked fiber lasers, Phys. Rev. A 85 (1) (2012) 013828.
[12] J.M. Soto-Crespo, Ph. Grelu, Nail Akhmediev, Dissipative rogue waves: Extreme pulses generated by passively mode-locked lasers, Phys. Rev. E 84 (1) (2011) 016604.
[13] Shanti Toenger, Thomas Godin, Cyril Billet, Frédéric Dias, Miro Erkintalo, Goëry Genty, John M. Dudley, Emergent rogue wave structures and statistics in spontaneous modulation instability, Sci. Rep. 5 (2015).
[14] Martin Golubitsky, Ian Stewart, The Symmetry Perspective, Springer, 2002.
[15] Edwin Ding, William H. Renninger, Frank W. Wise, Philippe Grelu, Eli Shlizerman, J. Nathan Kutz, High-energy passive mode-locking of fiber lasers, Int. J. Opt. 2012 (2012).
[16] L.M. Zhao, D.Y. Tang, T.H. Cheng, H.Y. Tam, C. Lu, 120nm bandwidth noise-like pulse generation in an erbium-doped fiber laser, Opt. Commun. 281 (1) (2008) 157–161.
[17] Dajun Lei, Hua Yang, Hui Dong, Shuangchun Wen, Huiwen Xu, Jinggui Zhang, Effect of birefringence on the bandwidth of noise-like pulse in an erbium-doped fiber laser, J. Modern Opt. 56 (4) (2009) 572–576.
[18] Cong Xu, Y.T. Dai, W. Li, H.X. Guo, Y. Zuo, K. Xu, J. Wu, J.T. Lin, Suppression of wave breaking in all normal dispersion (andi) fiber laser with a saturable absorber (sa), in: OptoeElectronics and Communications Conference (OECC), 2011 16th, IEEE, 2011, pp. 794–795.
[19] L.M. Zhao, D.Y. Tang, Generation of 15-nj bunched noise-like pulses with 93-nm bandwidth in an erbium-doped fiber ring laser, Appl. Phys. B 83 (4) (2006) 553–557.
[20] Sergey Kobtsev, Sergey Kukarin, Sergey Smirnov, Sergey Turitsyn, Anton Latkin, Generation of double-scale femto/pico-second optical lumps in mode-locked fiber lasers, Opt. Express 17 (23) (2009) 20707–20713.
[21] Sergei V. Smirnov, Sergey M. Kobtsev, Sergei Vladimirovich Kukarin, Aleksei Vladimirovich Ivanenko, New regime of single-pulse lasing in fibre lasers with mode locking by nonlinear polarisation evolution, Quantum Electron. 42 (9) (2012) 781.

[22] Sergey Smirnov, Sergey Kobtsev, Sergey Kukarin, Aleksey Ivanenko, Three key regimes of single pulse generation per round trip of all-normal-dispersion fiber lasers mode-locked with nonlinear polarization rotation, Opt. Express 20 (24) (2012) 27447–27453.
[23] D. Tang, L. Zhao, B. Zhao, Soliton collapse and bunched noise-like pulse generation in a passively mode-locked fiber ring laser, Opt. Express 13 (7) (2005) 2289–2294.
[24] Govind P. Agrawal, Nonlinear Fiber Optics, Academic Press, 2007.
[25] Oleg V. Sinkin, Ronald Holzlöhner, John Zweck, Curtis R. Menyuk, Optimization of the split-step fourier method in modeling optical-fiber communications systems, J. Lightwave Technol. 21 (1) (2003) 61.
[26] Stephen M. Hammel, James A. Yorke, Celso Grebogi, Do numerical orbits of chaotic dynamical processes represent true orbits? J. Complexity 3 (2) (1987) 136–145.
[27] George E.P. Box, Gwilym M. Jenkins, Gregory C. Reinsel, Time Series Analysis: Forecasting and Control, John Wiley & Sons, 2013.